

Numerical Simulation of Co-Flow Jet Airfoil Flows

Ge-Cheng Zha*, Wei Gao† Craig Paxton‡
Dept. of Mechanical and Aerospace Engineering
University of Miami
Coral Gables, Florida 33124
gzha@miami.edu

Abstract

A CFD calculation strategy is developed to simulate 2D co-flow jet airfoil. The jet ducts reaction forces are added to the surface integral of pressure and shear stress to calculate the total lift and drag. The predicted lift and drag agree well with the experiment at low angle of attack(AoA) and deviate largely at high AoA. The stall AoA of the CFJ airfoil is predicted reasonably well. Details of the flow field results and comparison between the computation and experiment are given in the paper.

1 Introduction

Flow control plays an important role to improve aircraft aerodynamic performance[1][2]. For different missions, different flow control methods may be used to achieve the required performance. For efficient cruise, the high ratio of lift to drag L/D is desirable. For short take off/landing(STOL) and high maneuverability, high lift and high stall angle of attack (not L/D) are the critical factors. For short landing distance, the high lift and high drag are desirable. So far, the flow control methods used in aircraft are mostly to enhance lift in order to reduce take off and landing distance.

Ref. [3] gives several active lift enhancement approaches that integrate the propulsion and airframe systems and are tested by Boeing Company for STOL. They include the Internal Blown Flaps (IBF), Externally Blown Flaps(EBF), Upper Surface Blowing(USB), and Vectored Thrust(VT). With both EBF and USB, the hot air from the engine is used to blow on the wing lower and upper surface. Hence the heat resistant materials are needed to cover the wings, which will generate the weight penalty. The USB requires placing the engines above and forward of the wing, which makes it inefficient for transonic cruise. The IBF is based on the circulation control(CC) approach and makes use of the Coanda effect to enhance circulation and lift. The IBF introduces the blowing air from the engine and can create a large penalty to the engine system. The VT approach needs to carry the vectored nozzle and its control system, which has a weight penalty for the flying mission.

Recently, Zha et al. have developed a co-flow jet (CFJ) airfoil concept to enhance lift, reduce drag, and increase stall margin[4, 5, 4] with low energy expenditure. The co-flow jet airfoil has an injection slot near the leading edge and a suction slot near the trailing edge on the airfoil suction surface. A high energy jet is injected near leading edge tangentially and the same amount of mass

* Associate Professor

† Graduate Student

‡ Graduate Student, Current Address: Phantom Works, Boeing Company, Huntsville, AL

flow is sucked in near trailing edge. The turbulent shear layer between the main flow and the jet causes strong turbulence diffusion and mixing, which enhances lateral transport of energy from the jet to mainflow and allows the main flow to overcome severe adverse pressure gradient and remain attached at high angle of attack(AoA). The co-flow jet airfoil dramatically enhances lift, reduces drag and increases stall margin as demonstrated in the wind tunnel tests[5].

The suction is a necessary process as long as a flow control method uses jet injection due to the mass conservation law. The jet suction momentum will generate penalty to the drag and lift. For CFJ airfoil, the suction occurs on the airfoil suction surface. For an airfoil with injection only such as a CC airfoil, the suction occurs by taking the air from freestream through the aircraft engine. The control volume analysis given in [6] indicates that the CFJ airfoil avoids the ram and captured area drag of the airfoil with injection only. The measured performance of the CFJ airfoil has already included the suction penalty, which is offset by the significant circulation enhancement. Compared with the airfoil with injection only, the CFJ airfoil with both injection and suction yields stronger mixing, larger circulation, more filled wake, higher stall angle of attack, less drag, and more efficient energy expenditure.

Since the CFJ airfoil injects and draws the same amount of the jet flow, the jet mass flow can be recirculated through the engine instead of being dumped such as the CC airfoil. This can significantly reduce the penalty to the propulsion system. The CFJ airfoil uses internal flow blowing and suction. No heat resistance materials required by the EBF and USB are needed.

This paper is to simulate the CFJ airfoils using CFD with two objectives: 1) develop a CFD strategy to calculate the CFJ airfoil performance. A CFD approach used as an analysis tool is necessary for CFJ airfoil design.; 2) Understand more about the physics of the CFJ airfoil flow fields based on the detailed data of the CFD solutions.

2 The CFJ Airfoil Geometry

The airfoil geometry simulated in this paper are the CFJ airfoil design and tested in [7]. Fig.1 shows the baseline airfoil NACA0025, and two airfoils with co-flow jet slots. The chord length is 0.1527m and the span is 0.3m. The co-flow jet airfoils are named using the following convention; CFJ4dig-INJ-SUC, where 4dig is the same as NACA 4 digit convention, INJ is replaced by the percentage of the ratio of the injection slot to the chord length and SUC is replaced by the percentage of the ratio of the suction slot size to the chord length. For example, the CFJ0025-065-196 airfoil has the suction surface recessed 0.65% of the chord at the injection slot and 1.96% of the chord at the suction slot. The new suction surface shape is a smooth translation between an exact copy of the original suction surface placed at both the 0.65% and 1.96% depths. The slot inlet and exit are located at 7.11% and 83.18% of the chord from the leading edge. The slot inlet and exit faces are normal to the suction surface to ensure that the jet will be tangential to the main flow.

In the experiment, the high pressure flow is injected into the high pressure cavity and then goes through a metallic foam to make the injection jet uniform. The CFD simulation take the downstream interface of the foam as the injection inlet.

3 CFD Solver

The Fluent CFD software is used in this research to calculate the 2D and 3D CFJ airfoil flows. The governing equations are the Reynolds averaged 3D compressible Navier-Stokes (RANS) equations. The pressure based second order upwind scheme is used to evaluate the inviscid flux and central differencing is used for the viscous terms. The $k - \epsilon$ turbulence model with integration to the wall and pressure gradient effect is employed. The y_1^+ is in the order of 1. The $k - \epsilon$ model is selected due to its capability of taking into account of turbulent boundary layer history effect by solving the complete transport equations of k and ϵ , and the $k - \epsilon$ model is more capable than algebraic models to predict the separated flows, which occur when the airfoil stalls at high AoA.

The full turbulent boundary layer assumption is used and is consistent with the tripped boundary layer in the experiments. Mesh refinement study is conducted for a few selected points to ensure that the solutions are mesh size independent. Since the CFD solutions are obtained from the steady state calculations based on RANS model, the unsteady details of the shear layer mixing entrainment and large coherent vortex structures are not able to be captured.

The wind tunnel walls are included in the CFD simulation to consider the wind tunnel wall effect. The total pressure and total temperature are given at the wind tunnel inlet as the boundary conditions. The static pressure at wind tunnel exit is iterated to make the wind tunnel inlet Mach number match the experimental value. The total pressure and total temperature are also given at the injection duct inlet as the boundary conditions. The injection total pressure is iterated to match the experimental momentum coefficient. The static pressure at the suction duct entrance is iterated to match the injection jet mass flow rate.

As mentioned above, several layers iterations are needed to achieve a converged CFJ airfoil solution at a certain AoA. The calculation is thus very CPU intensive, in particular for 3D cases. The 2D CFJ airfoil calculation is therefore very desirable. The control volume analysis given in [6] provides formulations to calculate the lift and drag generated by the jet ducts.

4 Jet Reaction Forces

In [6], a control volume analysis gives the formulations to calculate the lift and drag contributed by the reaction forces generated by the injection and suction ducts.

The drag of a CFJ airfoil is:

$$D = R'_x - F_{x_{cfj}} = \int_h^b \rho V_e (V_\infty - V_e) dy \quad (1)$$

Or

$$D = \int_h^b \rho V_e (V_\infty - V_e) dy \quad (2)$$

Where R'_x is the drag from the airfoil surface integral of shear stress and pressure. $F_{x_{cfj}}$ is the drag due to the reaction forces generated by the injection and suction ducts and is:

$$F_{x_{cfj}} = (\dot{m}_{j1} u_{j1} + (p_{j1} A_{j1})_x) - (\dot{m}_{j2} u_{j2} + (p_{j2} A_{j2})_x)$$

$$= (\dot{m}_j V_{j1} + p_{j1} A_{j1}) * \cos(\theta_1 - \alpha) - (\dot{m}_j V_{j2} + p_{j2} A_{j2}) * \cos(\theta_2 + \alpha) \quad (3)$$

Where, the θ is the angle between the slot surface and the line normal to the airfoil chord. For the CFJ0025-065-196 airfoil[7], $\theta_1 = 25.86^\circ$, $\theta_2 = 14.31^\circ$, α is the angle of attack, V_j is the jet velocity, p_j is the jet static pressure, \dot{m}_j is the jet mass flow rate, A_j is the jet slot area.

For a CFJ airfoil, the wind tunnel measured drag is the actual drag that the aircraft will experience. This is different from an airfoil with injection only such as a circulation control airfoil[6]. For an airfoil with injection only, the actual drag, or equivalent drag, is the drag measured in wind tunnel plus the drag due to the suction of the jet mass from the freestream, which includes the ram drag and captured area drag. The reason for the difference between a 2D CFJ airfoil and the airfoil with injection only is: for the 2D CFJ airfoil, the mass conservation is satisfied due to recirculating the jet; for the airfoil with injection only such as a circulation control airfoil, the 2D airfoil does not satisfy the mass conservation since there is no source for the jet injection.

The lift of a CFJ airfoil is:

$$L = R'_y - F_{y_{cfj}} \quad (4)$$

Where R'_y is the y-direction component of the surface pressure and shear stress integral, which is primarily induced by the circulation. $F_{y_{cfj}}$ is the jet ducts reaction force component in y-direction.

$$\begin{aligned} F_{y_{cfj}} &= (\dot{m}_{j1} v_{j1} + (p_{j1} A_{j1})_y) - \gamma(\dot{m}_{j2} v_{j2} + (p_{j2} A_{j2})_y) \\ &= (\dot{m}_j V_{j1} + p_{j1} A_{j1}) * \sin(\theta_1 - \alpha) + \gamma(\dot{m}_j V_{j2} + p_{j2} A_{j2}) * \sin(\theta_2 + \alpha) \end{aligned} \quad (5)$$

The CFD procedure to calculate the lift and are is: 1) calculate the surface integrals of the pressure and shear stress R'_x and R'_y ; 2) calculate the jet ducts reaction forces, $F_{x_{cfj}}$ and $F_{y_{cfj}}$; 3) calculate the total drag and lift based on Eqs. (1) and (4).

5 Results and Discussion

Figure 2 is the zoomed 2D mesh near the CFJ0025-065-196 airfoil. The structured mesh is used around the airfoil and unstructured mesh is used in the region away from the airfoil where the flow gradient is small. The total number of cells is 170k. The freestream Mach number is about 0.1 and the Reynolds number based on chord is 380k. The flow is assumed normal to the injection duct inlet. The suction duct is only simulated with an entrance opening since the flow inside the suction duct has little effect on the flow outside of the suction duct. Simulation of the injection duct gives a more realistic injection mixing effect when the jet enters into the mainflow.

Fig.3 is the computed injection momentum coefficient compared with the experiment for CFJ0025-065-196 airfoil at different angle of attack. The momentum coefficients are iterated in the computation and they agree well with the experiment. The cases computed correspond to the experimental cases with the total pressure coefficient of 1.27[7]. The total pressure coefficient is defined as the ratio of the injection total pressure to the freestream total pressure. In the experiment, the injection total pressure is held constant while the AoA is varying.

Figure 4 is the computed lift coefficient compared with the experiment. The two bold lines are the experiment of the CFJ airfoil and the baseline airfoil. The CFJ airfoil has increased maximum

lift by 220% and stall margin by 153%. The predicted baseline airfoil lift (open triangle symbols) agrees fairly well with the experiment (solid triangle symbols), except that the predicted stall AoA is about 3 degree higher than the experiment. For the CFJ0025-065-196 airfoil, the predicted lift coefficient is in good agreement with the experiment up to AoA=20°. When the AoA is greater than 20°, the computation under-predicts the lift significantly. The large discrepancy may be due to the inherent unsteadiness of the mixing process at high AoA under large adverse pressure gradient. The RANS model used in this paper may be not adequate to capture the unsteady mixing process, which could have large vortex structure such as the coherent vortices due to the jet dissimilarity and Görtler vortices caused by the surface curvature.

Figure 5 is the computed drag coefficient compared with the experiment. The two bold lines are the measured drag coefficient of the CFJ airfoil and the baseline airfoil. The CFJ airfoil has lower drag than the baseline airfoil before the baseline airfoil stalls. At zero angle of attack, the CFJ airfoil has negative drag, that is thrust. The CFD slightly under-predicts the baseline airfoil drag coefficient when $\text{AoA} \leq 10^\circ$. The predicted drag coefficient remains flat at high AoA for the baseline airfoil, whereas the measured drag coefficient increases significantly at high AoA. The discrepancy of the baseline airfoil drag prediction is hence increased at high AoA. The predicted CFJ airfoil drag coefficient agrees fairly well when the $\text{AOA} \leq 10^\circ$. Similar to the baseline airfoil, the drag of the CFJ airfoil remains flat at high angle of attack and is significantly under-predicted. This again may be due to the inadequacy of the RANS turbulence model to simulate the flow mixing at high angle of attack.

Figure 6 is the computed wake of the baseline and CFJ airfoil at AoA=10° measured one chord downstream of the trailing edge. The baseline airfoil has a deep velocity deficit, whereas the CFJ airfoil has a reversed velocity deficit. The wake deficit determines the total drag as indicated by Eq.(2). For the CFJ airfoil, Fig. 6 shows that the airfoil will have a negative drag, or a thrust.

Figure 6 shows the wake profiles at AoA of 0°, 10°, 20°, and 39°. The wake velocity has a reversed deficit at AoA = 0°. Such reversed deficit is weakened at AoA = 10°. A shallow velocity deficit appears at AoA = 20°. A deep velocity deficit is formed at AoA = 39° due to the large AoA. This trend reflects that the drag will vary from a thrust at low AoA to a large drag at high AoA.

Figure 8 plots the surface isentropic Mach number of the baseline and CFJ0025-065-196 airfoil at AoA=10°. The overall loading of the CFJ airfoil is much higher than that of the baseline airfoil, which indicates that the CFJ airfoil has a much higher circulation. The higher circulation is also reflected by the more downstream leading edge stagnation point. The CFJ airfoil also has higher leading edge suction peak Mach number, which generates the low pressure at LE and results in a thrust.

Figure 9 and 10 are the flow visualization of the baseline airfoil at AoA = 10° and 20°[7]. It shows that the baseline airfoil has attached flow at AoA = 10° and has a massive separation at AoA = 20°. Figure 11 and 12 show the computed Mach number contours at AoA = 10° and 20°, which correctly captures the attached flow at AoA = 10° and massively separated flow at AoA = 20°.

Figure 13 and 14 show the Mach contours and streamlines at AoA = 43° measured by the PIV system in the wind tunnel tests[7]. The flow is attached at AoA = 43°. Figure 15 and 16 are the Mach contours and streamlines computed by CFD. The computed results show that the flow is at the verge of separation at AoA = 43°. The computed flow field at AoA = 39° with the flow fully attached is more like the experimental flow field at AoA = 43°.

Figure 17 and 18 are the Mach contours and streamlines at AoA = 46° measured by the PIV

system in the wind tunnel tests[7]. The flow is massively separated at $\text{AoA} = 46^\circ$. Figure 19 is the Mach contours and streamlines computed by CFD at $\text{AoA} = 45^\circ$ and shows a massive separation. Overall, the CFJ airfoil separation AoA predicted by CFD agrees reasonably well with the experiment.

6 Conclusions

A CFD simulation is conducted for 2D co-flow jet airfoil with $k - \epsilon$ turbulence model. The jet ducts reaction forces are added to the surface integral of pressure and shear stress to calculate the total lift and drag. The computed lift and drag agree well with the experiment at low angle of attack(AoA) and are significantly under-predicted at high AoA . The predicted wake profile has reversed velocity deficit at low AoA , which is consistent with the experiment that a thrust is generated at low AoA . When the AoA is high, the wake becomes deep and the drag is increased. The predicted isentropic Mach number indicates a much larger circulation of the CFJ airfoil than that of the baseline airfoil. The AoA that causes the massive separation of CFJ airfoil is predicted well.

References

- [1] M. Gad-el Hak, "Flow Control: The Future ," *Journal of Aircraft*, vol. 38, pp. 402–418, 2001.
- [2] M. Gad-el Hak, *Flow Control, Passive, Active, and Reactive Flow Management*. Cambridge University Press, 2000.
- [3] T. C. Corke, *Design of Aircraft*. Prentice Hall, 2003.
- [4] G.-C. Zha and C. Paxton, "A Novel Airfoil Circulation Augment Flow Control Method Using Co-Flow Jet." NASA/CP-2005-213509, June 2005; AIAA Paper 2004-2208, June 2004.
- [5] G.-C. Zha and D. C. Paxton, "A Novel Flow Control Method for Airfoil Performance Enhancement Using Co-Flow Jet." *Applications of Circulation Control Technologies*, Progress in Astronautics and Aeronautics, AIAA Book Series, Editors: Joslin, R. D. and Jones, G.S., to be published in 2006.
- [6] G.-C. Zha and W. Gao, "Analysis of Jet Effects on Co-Flow Jet Airfoil Performance with Integrated Propulsion System." AIAA Paper 2006-0102, 2006.
- [7] G.-C. Zha, B. Carroll, C. Paxton, A. Conley, and A. Wells, "High Performance Airfoil with Co-Flow Jet Flow Control." AIAA-Paper-2005-1260, Jan. 2005, submitted for publication in AIAA Journal.

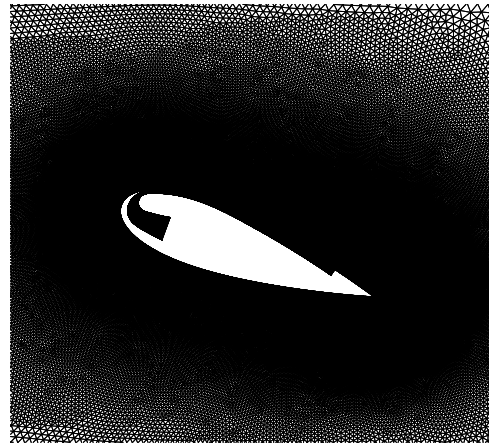
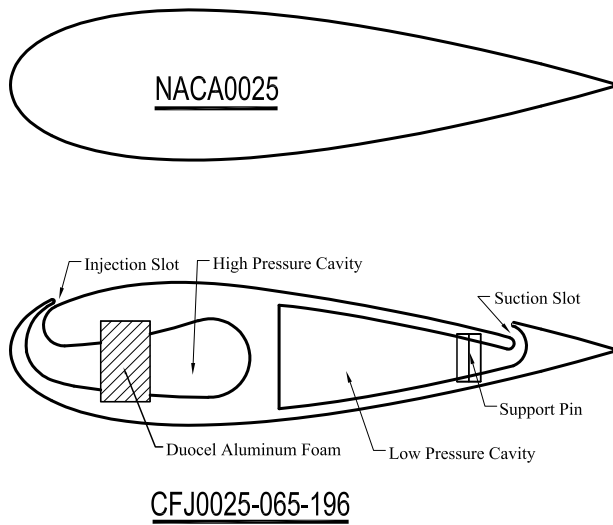


Figure 2: Zoomed 2D CFD mesh around CFJ0025-065-196 airfoil.

Figure 1: Baseline airfoil of NACA0025 and the CFJ airfoil of CFJ0025-065-196.

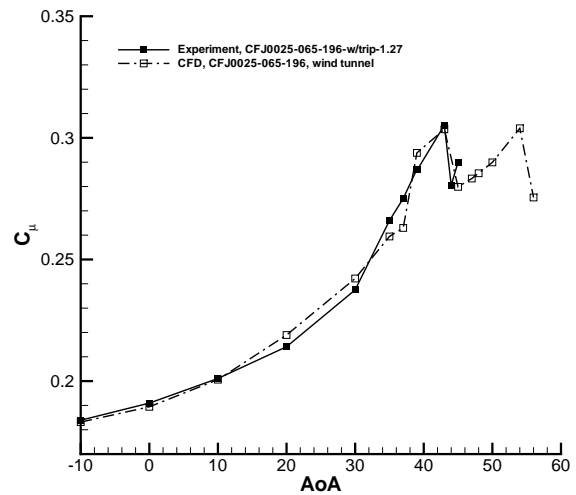


Figure 3: Computed injection momentum coefficient compared with wind tunnel test results.

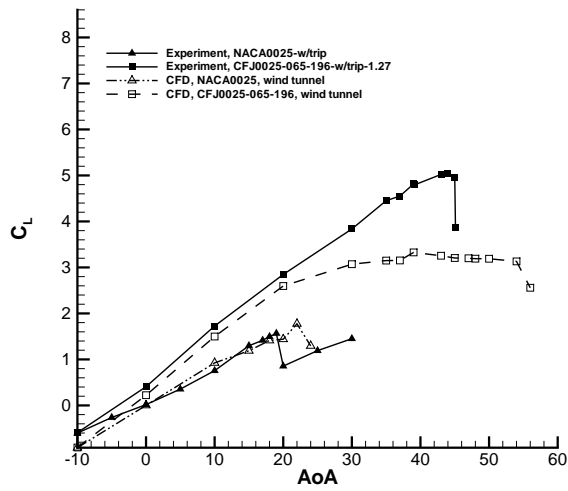


Figure 4: Computed lift coefficient compared with wind tunnel test results.

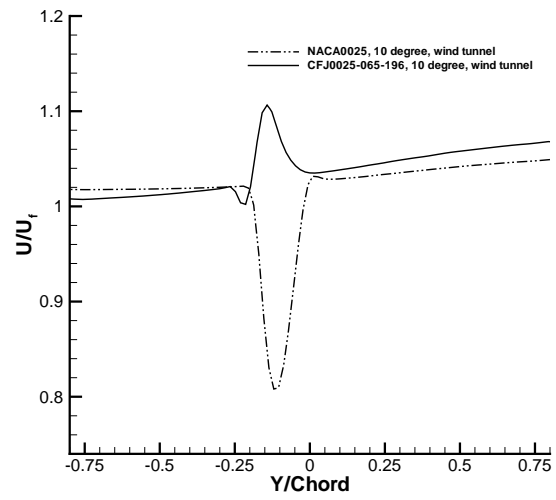


Figure 6: Computed CFJ airfoil wake shape compared with the baseline airfoil at AoA=10 degrees.

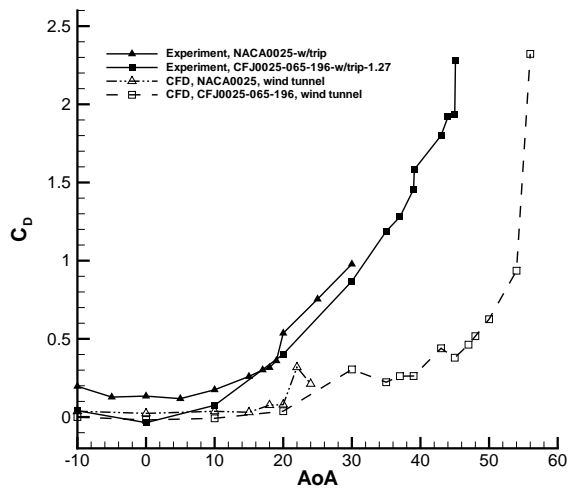


Figure 5: Computed drag coefficient compared with wind tunnel test results.

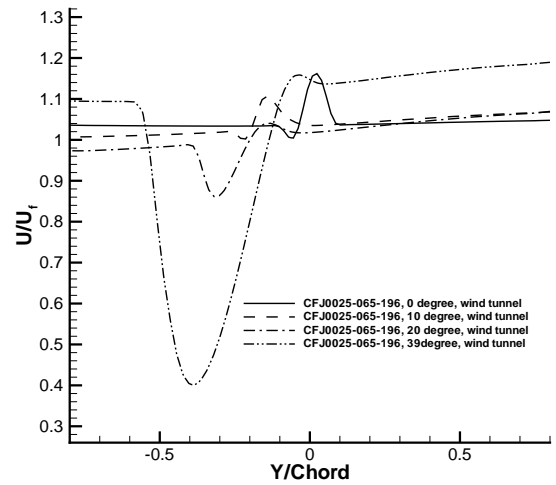


Figure 7: Computed CFJ airfoil wake shape compared with the baseline airfoil at different AoA.

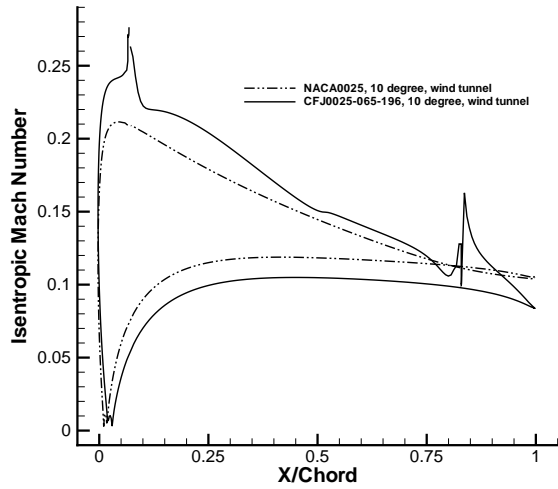


Figure 8: Computed airfoil surface isentropic Mach number distribution at AoA=10°.

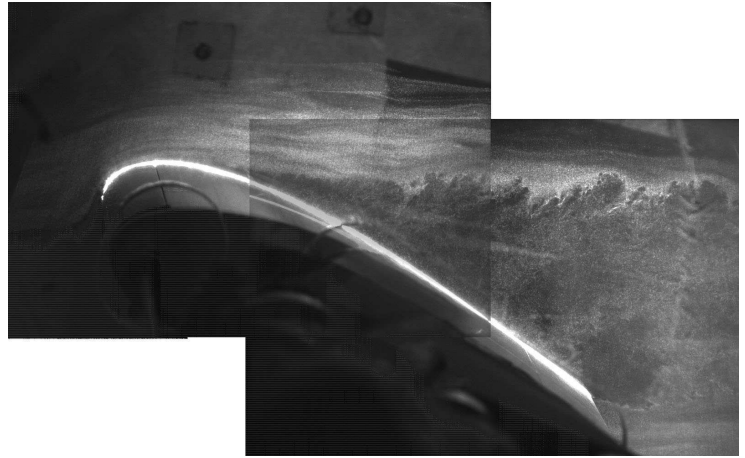


Figure 10: Flow visualization of the separated flow of baseline NACA0025 airfoil at AoA of 20°.

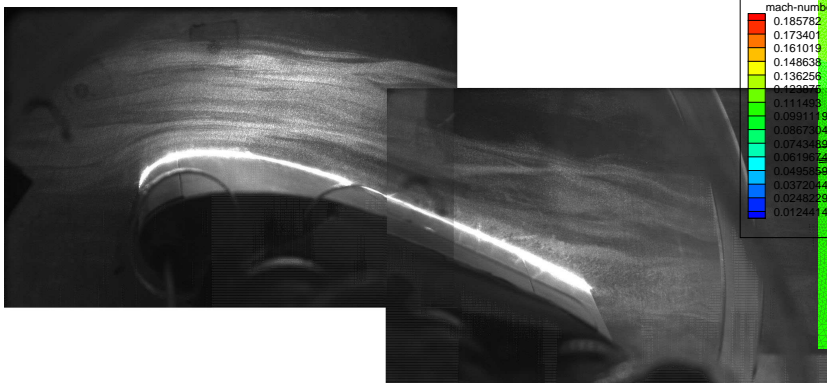


Figure 9: Flow visualization of the attached flow of baseline NACA0025 airfoil at AoA of 10°.

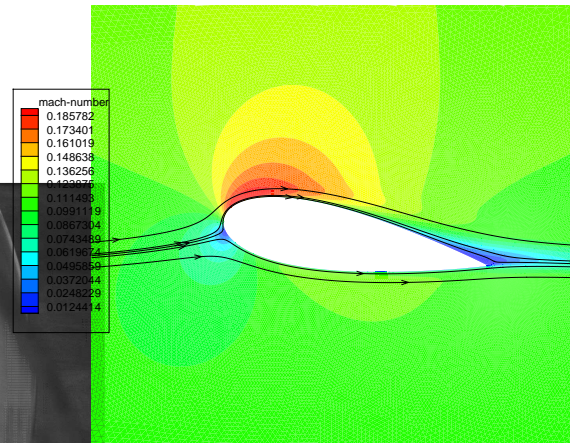


Figure 11: Computed NACA0025 baseline airfoil Mach contours with streamlines at AoA=10°.

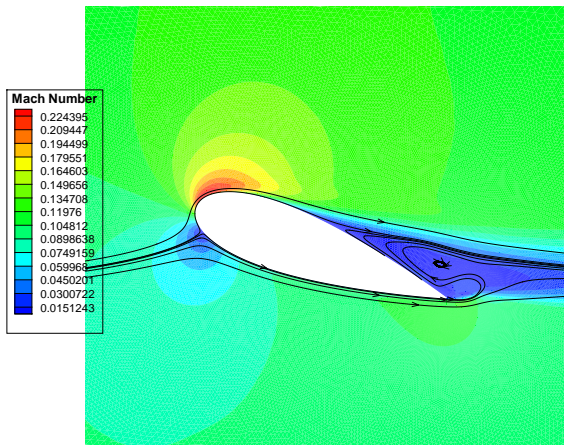


Figure 12: Computed NACA0025 baseline airfoil Mach contours with streamlines at AoA=20°.

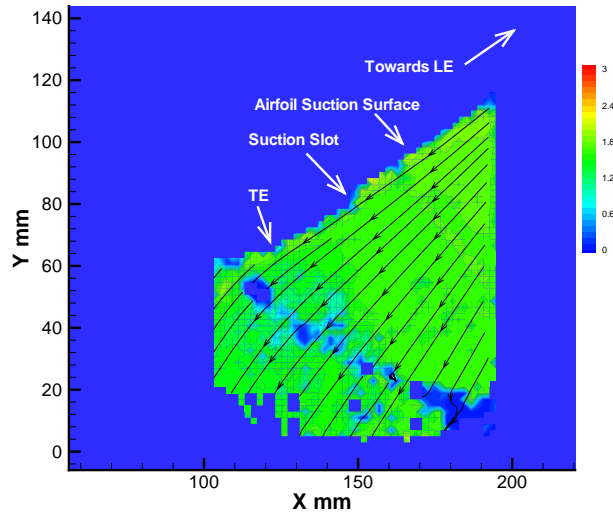


Figure 14: PIV measured normalized velocity (V/V_∞) contours and streamlines of the attached flow of CFJ0025-065-196 airfoil at AoA of 43°, rear portion.

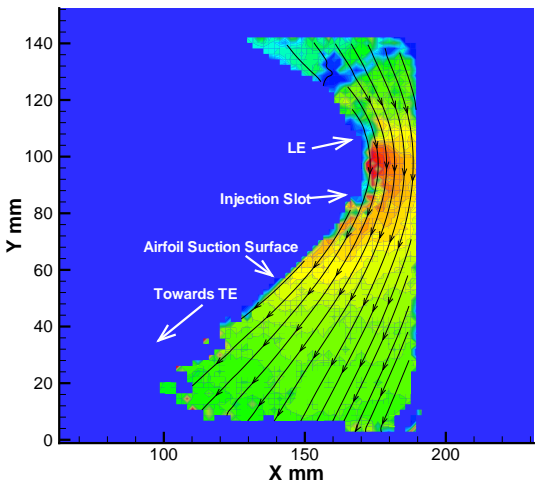


Figure 13: PIV measured normalized velocity (V/V_∞) contours and streamlines of the attached flow of CFJ0025-065-196 airfoil at AoA of 43°, front portion.

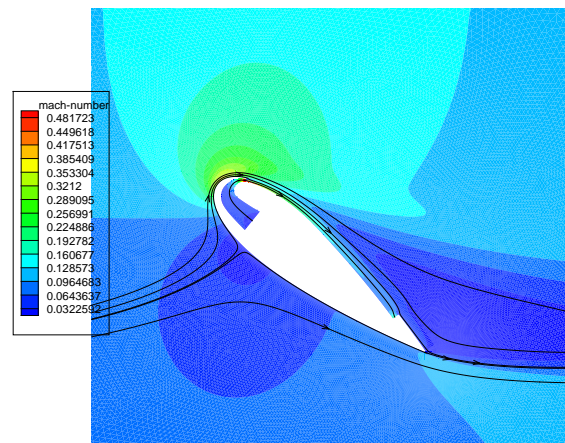


Figure 15: Computed CFJ airfoil Mach contours with streamlines at AoA=39°.

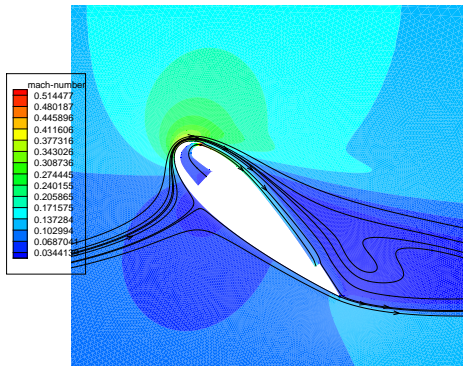


Figure 16: Computed CFJ airfoil Mach contours with streamlines at AoA=43°.

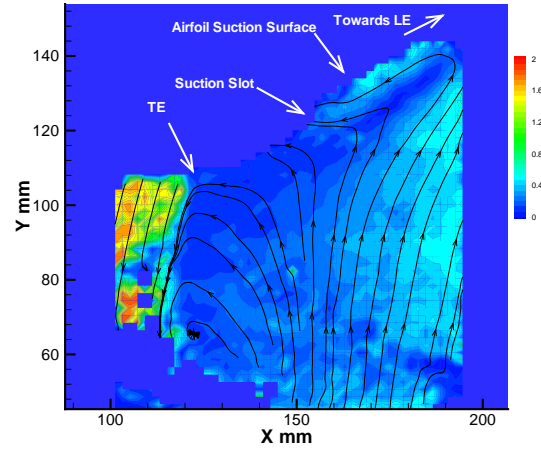


Figure 18: PIV measured normalized velocity (V/V_∞) contours and streamlines of the separated flow of CFJ0025-065-196 airfoil at AoA of 46°, rear portion.

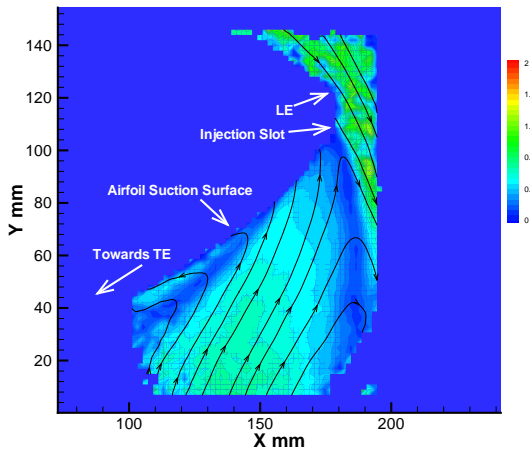


Figure 17: PIV measured normalized velocity (V/V_∞) contours and streamlines of the separated flow of CFJ0025-065-196 airfoil at AoA of 46°, front portion.

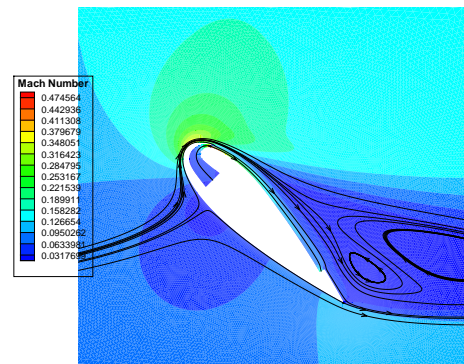


Figure 19: Computed CFJ airfoil Mach contours with streamlines at AoA=45°.